Pulmonary arterial hypertension reduces energy efficiency of right, but not left, rat ventricular trabeculae

Toan Pham[1,2], Linley Nisbet[1,2], Andrew Taberner[1,3], Denis Loiselle[1,2], June-Chiew Han[1]

[1]Auckland Bioengineering Institute, [2]Department of Physiology,
[3]Department of Engineering Science, The University of Auckland, Auckland, New Zealand

Running title: Ventricular energetics in pulmonary arterial hypertension

Key Words: Right heart failure, cardiac efficiency, cardiac activation heat

Corresponding Author: Toan Pham, Auckland Bioengineering Institute, The University of Auckland, Auckland, 1010, New Zealand

Email: tpha025@aucklanduni.ac.nz

Toan Pham received his MSc degree in Biological Science from the University of Auckland, Auckland, New Zealand in 2013. He is currently pursuing the PhD degree in Physiology at the same university. His research interest is in cardiac muscle physiology, particularly focussing on cardiac energetic efficiency at the tissue and subcellular (mitochondria) levels in health and disease.

This is an Accepted Article that has been peer-reviewed and approved for publication in the The Journal of Physiology, but has yet to undergo copy-editing and proof correction. Please cite this article as an 'Accepted Article'; doi: 10.1113/JP275578.

Table of Contents Category: Cardiovascular

Key points summary:

- Pulmonary arterial hypertension (PAH) triggers right-ventricular (RV) hypertrophy and left-ventricular (LV) atrophy, which progressively leads to heart failure.
- We designed experiments under conditions mimicking those encountered by the heart *in vivo* that allowed us to investigate whether consequent structural and functional remodelling of the ventricles affects their respective energy efficiencies.
- We found that peak work output was lower in RV trabeculae from PAH rats, due to reduced extent and velocity of shortening. However, their suprabasal enthalpy was unaffected due to increased activation heat, resulting in reduced suprabasal efficiency. There was no effect of PAH on LV suprabasal efficiency.
- We conclude that the mechanism underlying the reduced energy efficiency of hypertrophied RV tissues is attributable to the increased energy cost of Ca^{2+} cycling, whereas atrophied LV tissues still maintained normal mechano-energetic performance.

Abstract

Pulmonary arterial hypertension (PAH) greatly increases the afterload on the right ventricle (RV), triggering RV hypertrophy, which progressively leads to RV failure. In contrast, the disease reduces the passive filling pressure of the left ventricle (LV), resulting in LV atrophy. We investigated whether these distinct structural and functional consequences to the ventricles affect their respective energy efficiencies. We studied trabeculae isolated from both ventricles of Wistar rats with monocrotaline-induced PAH and their respective Control groups. Trabeculae were mounted in a calorimeter at 37 °C. While contracting at 5 Hz, they were subjected to stress-length work-loops over a wide range of afterloads. They were subsequently required to undergo a series of isometric contractions at various muscle lengths. In both protocols, stress production, length change, and suprabasal heat output were simultaneously measured. We found that RV trabeculae from PAH rats generated higher activation heat, but developed normal active stress. Their peak external work output was lower due to reduced extent and velocity of shortening. Despite lower peak work output, suprabasal enthalpy was unaffected, thereby rendering suprabasal efficiency lower. Crossbridge

efficiency, however, was unaffected. In contrast, LV trabeculae from PAH rats maintained normal mechano-energetic performance. Pulmonary arterial hypertension reduces the suprabasal energy efficiency of hypertrophied right-ventricular tissues, as a consequence of the increased energy cost for Ca^{2+} cycling.

Introduction

Pulmonary arterial hypertension (PAH) is an incapacitating disease. If untreated, its mortality rate of 40 % (Sitbon *et al.*, 2002; Humbert *et al.*, 2010) three years post-diagnosis remains extreme. Death results primarily from right heart failure (van Wolferen *et al.*, 2007; Campo *et al.*, 2010). This is because the increased pulmonary vascular resistance and resulting elevated pulmonary artery pressure impose a high afterload on the right ventricle (RV), inducing sustained pathological RV hypertrophy, which ultimately leads to RV failure (Vonk-Noordegraaf *et al.*, 2013). In addition to RV structural remodelling, PAH patients suffer a constellation of RV systolic abnormalities: lower ejection fraction (Gan *et al.*, 2006; Rain *et al.*, 2013), lower stroke volume (Marcus *et al.*, 2001; Gan *et al.*, 2006; Schafer *et al.*, 2009), and reduced peak systolic strain and strain rate (Li *et al.*, 2013). A comprehensive study by Wong *et al.* (2011) comparing two cohorts of PAH patients (NYHA Class II and Class III), showed markedly reduced myocardial energy efficiency of the RV owing to increased myocardial oxygen consumption.

A widely-studied rat model induces PAH by a single injection of monocrotaline (MCT). This agent selectively damages the vascular endothelium of the lung, causing a series of RV pathological changes that are consistent with those seen in PAH patients (Hardziyenka *et al.*, 2011; Hardziyenka *et al.*, 2012). Using isolated RV papillary muscles obtained from such a PAH rat model, Wong *et al.* (2010) showed increased oxygen consumption and hence reduced efficiency – results that are in striking accord with those from their study of human patients (Wong *et al.*, 2011). The consistency of these findings between the animal and patient studies clearly implicates disturbance of energy utilisation in the aetiology of PAH.

Nevertheless, the mechanism underlying RV energy disturbance in PAH remains unknown. This uncertainty provides the primary aim of the present study. We hypothesise that the observed energy disturbance in RV myocardium in PAH arises from a shift towards high energy costs of both crossbridge cycling and Ca^{2+} cycling. Our hypothesis stems from various lines of evidence: (i)

disruption of the transverse tubular network (Xie *et al.*, 2012), (ii) prolongation of the action potential (Lee *et al.*, 1997; Piao *et al.*, 2010; Hardziyenka *et al.*, 2012), (iii) prolongation of the Ca^{2+} transient (Lamberts *et al.*, 2007; Miura *et al.*, 2011; Lookin *et al.*, 2015), and (iv) decreased expression of the sarcoplasmic reticular ATPase (Kogler *et al.*, 2003; Hardziyenka *et al.*, 2011; Hadri *et al.*, 2013). Experimental testing our hypothesis is designed to provide an explanation for the reported decreased RV mitochondrial energy-producing ability (Redout *et al.*, 2007; Daicho *et al.*, 2009; Wust *et al.*, 2016) and the resulting myocardial contractile dysfunction observed in PAH RV tissue preparations (Korstjens *et al.*, 2002; Miura *et al.*, 2011; Lookin *et al.*, 2015).

A secondary aim of our study was to investigate whether energy disturbance also presents in the myocardium of the left ventricle (LV) as a consequence of PAH. Over the past decade, the importance of 'ventricular interdependence' (Hsia & Haddad, 2012; Naeije & Badagliacca, 2017) has been demonstrated in the PAH disease setting. This high degree of ventricular interdependency means that, as the RV undergoes hypertrophy, the septal constantly bows leftward. Thus LV diastolic filling is greatly reduced, subsequently leading to LV atrophic remodelling (Vonk-Noordegraaf *et al.*, 2005; Gan *et al.*, 2006; Marcus *et al.*, 2008). A number of studies have reported several anomalies in the LV myocardium during PAH. These include reduction of peak LV systolic pressure (Correia-Pinto *et al.*, 2009), prolongation of action potential (Hardziyenka *et al.*, 2012), lower longitudinal conduction velocity (Hardziyenka *et al.*, 2012), and a shift of myosin heavy chain (MHC) profile from the fast to the slow isoform (Lowes *et al.*, 1997; Correia-Pinto *et al.*, 2009). Nevertheless, whether these contractile and ionic dysfunctions are associated with disturbed LV energy utilisation is unknown. We hypothesise that PAH disturbs LV energy utilisation such that LV efficiency is also reduced.

To test these two hypotheses, we have investigated energy efficiency using isolated trabeculae from both ventricles of MCT-treated and Control rats. Different energy expenditure sources (crossbridge and Ca^{2+} cycling-related metabolism) were partitioned using two protocols: isometric pre-shortened and afterloaded isotonic work-loops. We measured heat as a proxy of oxygen consumption, and experiments were performed over a wide range of afterloads. We chose isolated cardiac trabeculae because of the linear arrangement of their cardiomyocytes along the longitudinal axis, unlike the multi-orientated fiber directions of the whole-heart. Unlike papillary muscles, trabeculae are sufficiently thin to obviate the risk of hypoxia during high metabolic demand (Han *et al.*, 2011), which is an important factor to consider since we challenge them at high afterloads to mimic the hypertensive condition.

Methods

Ethical Approval

Experiments were conducted in accordance with protocols approved by the University of Auckland Animal Ethics Committee (R1403) and conform to principles and regulations described in a *Journal of Physiology* Editorial (Grundy, 2015).

Animal model

Male Wistar rats (300 g – 325 g) received either a single subcutaneous injection of monocrotaline (MCT, Sigma Aldrich, 60 mg kg^{-1}) as the PAH group (n = 26) or an equivalent volume of saline as the Control group (n = 20). Treated animals had *ad libitum* access to standard rat chow and water, and experienced a 12 hr light/dark environment. They were weighed three times a week for the first 4 weeks, but daily thereafter for another 2 weeks. The latter frequency was necessary as we observed that the MCT-treated rats began to show several phenotypical signs of RV failure, including laboured respiration, lethargy, ruffled fur and lack of inquisitiveness, but most importantly, they started to experience consecutive days of body weight loss (>15%, a criterion for end-stage RV failure). A previous study from our laboratory has reported that the PAH rats, commencing at Week 4 post-injection, show pronounced cardiac hemodynamic changes *in vivo*. These include decreased heart rate, decreased mean arterial blood pressure and, most importantly, a 3-fold increase in RV systolic pressure (Han *et al.*, 2017).

Muscle preparation

Not later than post-injection Week 6, each rat was deeply anaesthetised with isoflurane and weighed before injecting with heparin (1000 IU kg^{-1}). Following cervical dislocation, the heart was rapidly excised and plunged into cold Tyrode solution and immediately Langendorff-perfused with oxygenated Tyrode solution (at room temperature), which contained (in mmol L^{-1}): 130 NaCl, 6 KCl, 1 $MgCl_2$, 0.5 NaH_2PO_4, 0.3 $CaCl_2$, 10 HEPES, 10 glucose and 20 2,3-butanedione monoxime (BDM) with pH adjusted to 7.4 using Tris.

Under a dissecting microscope, intact trabeculae were dissected from the endocardial surfaces of both left and right ventricles. A suitable trabecula, in terms of its geometrical uniformity and small diameter to enhance diffusive oxygen supply, was transferred to a work-loop calorimeter (Taberner *et al.*, 2015) and mounted between two platinum hooks connected to a custom-built force

transducer at the downstream end and a length motor at the upstream end. In the calorimeter, the muscle was superfused with the same oxygenated Tyrode solution as used during dissection, except at a higher concentration of $CaCl_2$ (1.5 mmol L^{-1}) and in the absence of BDM. The superfusate was pH Tris-adjusted to 7.4 at body temperature (37 °C). The rate of flow of Tyrode superfusate over the muscle in the measurement chamber was electronically maintained at 0.55 µL s^{-1} (Taberner *et al.*, 2017). This flow rate provides adequate oxygenation to the muscle (Han *et al.*, 2011) while maximising the thermal signal-to-noise ratio (Johnston *et al.*, 2015).

Once mounted and superfused, the trabecula was electrically stimulated to contract at 3 Hz (via platinum electrodes in the measurement chamber) for at least 1 hr before it was gradually stretched to optimal length (L_o; the length that maximises developed force). The length of the trabecula was measured at L_o in the calorimeter, as was its diameter in two orthogonal views via a 45° mirror, using a microscope graticule. Since each studied trabecula resembled an ellipse in cross-section (Goo *et al.*, 2009), cross-sectional areas were calculated from the two orthogonal measurements of major and minor diameters.

The force developed by the trabecula was determined by a laser interferometer system, using a custom-made, low-compliance transducer, while its length was controlled using a motor under software control. The rate of muscle suprabasal heat production was measured and quantified from the difference in temperature between down-stream and up-stream thermopile arrays and the flow-rate-dependent temperature sensitivity (Taberner *et al.*, 2011). The entire calorimeter system was then optically-isolated and thermally-insulated in an enclosure to ensure that the environmental temperature was maintained at 37 °C.

Experimental protocols

A period of about 1 hour was required to gradually increase the temperature of the calorimeter to 37 °C, during which time muscle force and rate of suprabasal heat production both reached steady-states. Experiments were performed with the trabecula contracting at 5 Hz to mimic the physiological heart rate of the rat. Each trabecula was first required to contract isometrically, where its length was servo-maintained using the upstream length motor. The trabecula was subsequently required to undergo force-length work-loop contractions, preloaded at L_o, at six different afterloads. Each afterloaded work-loop reached a steady state of force and heat output after 2-3 min. The muscle was returned to isometric contractions between each bout of work-loops to allow comparison of the baselines of the rates of suprabasal heat production at different afterloads. Isotonic work-loop contractions approximate the pressure-volume loops of the heart, thereby

allowing measurements of stress-length work output, suprabasal enthalpy, and suprabasal efficiency, as well as both the extent and velocity of contraction.

Upon completion of the work-loop protocol experiments, the trabecula was then required to undergo a series of isometric contractions at different preloads, in which muscle length was progressively reduced, in 5 steps, from L_o to L_{min} (the length at which negligible macroscropic active force was observed). Electrical stimulation was halted for 3 min between each length step transition to provide baselines for zero force and zero active heat.

Post-experiment quantifications

The heat artifact resulting from the small cyclic movement (up to about 0.3 mm) of the upstream hook (required to change muscle length during work-loop contractions) was quantified by oscillating the hook at a frequency of 5 Hz at the extent of muscle shortening achieved at the lowest afterload while the muscle was quiescent. A second heat artefact, resulting from electrical stimulation at 5 Hz, was quantified in the absence of a muscle. Net muscle heat output was calculated by subtracting these two artefactual sources of heat, which typically averaged at most 10 % of maximal active heat.

Upon completion of an experiment, the thickness of the ventricular free wall was measured using a dissecting microscope graticule. Tibial length of the rat was measured, and the heart (including the dissected trabeculae) and lungs dried in an oven at 60 °C for at least 24 hr prior to weighing.

Definitions

Measurements of force, length, and rate of heat output were acquired using LabVIEW software (National Instruments, Austin, USA) and analysed offline using a custom-written MATLAB (MathWorks, Natick, MA, USA) program. Force was converted to stress (kPa) by normalising to muscle cross-sectional area. Twitch duration was quantified at 5 % and 50 % of peak active stress. Twitch heat (kJ m^{-3}) was calculated by dividing the steady-state rate of heat production by the stimulus frequency (5 Hz) and normalizing it to muscle volume. Relative active stress is the ratio of active stress, at which the muscle transitioned from isometric phase to isotonic shortening, to the peak isometric active stress at L_o. External work output (kJ m^{-3}) was calculated by integrating stress as function of relative muscle length over the period of the twitch. Suprabasal enthalpy (kJ m^{-3}) was calculated as the sum of work and suprabasal heat. Suprabasal efficiency was defined as the ratio of work to suprabasal enthalpy. Crossbridge efficiency was defined as the ratio of work to crossbridge enthalpy (following subtraction of the activation heat from the suprabasal enthalpy). Relative extent of shortening (%) was given by the distance that the muscle shortened during the isotonic phase at

each afterloaded work-loop) normalised to L_o. Velocity of shortening (s^{-1}) was calculated as the maximal slope of the relative length-time trace during the isotonic phase of work-loop. Heat-stress relations were fitted using linear regression for each muscle. Activation heat was defined as the averaged heat-intercept of the heat-stress relations arising from the isometric contractions. Peak 'shortening heat' was calculated as the difference between the heat-intercepts from the work-loop (shortening) and isometric (non-shortening) protocols.

Statistical Analyses

Measured variables were plotted as functions of either relative muscle length or stress (afterload). Data were fitted using polynomial regression (up to third-order) and the regression lines were averaged within groups using the 'random coefficient model' (a 'Maximum Likelihood' curve-fitting technique advocated by Feldman (1988)) within PROC MIXED of the SAS software package (SAS Institute Inc., Cary, NC, USA). For clarification, as illustrated in Figure 7A, there are 16 fitted regression lines (thin lines) representing 16 Control LV trabeculae; the resulting average line (thick line) is superimposed.

Suitable trabeculae could not always be found in both ventricles from the same heart. In Control rats, 6 hearts each provided 1 LV and 1 RV trabeculae, 12 hearts each provided 1 trabecula from either ventricle, and 3 hearts each provided 2 RV trabeculae. In MCT-treated rats, 9 hearts each provided 1 LV and 1 RV trabeculae, 3 hearts each provided 1 LV and 2 RV trabeculae, 12 each hearts provided 1 trabecula from either ventricle, and 2 hearts each provided 2 RV trabeculae. In consequence, a nested design in which trabeculae were nested within hearts was adopted.

The significance of differences among regression lines, or peak mean values, of the four groups was tested for the effect of PAH both between ventricles (LV versus RV) and within ventricles (Control versus PAH) using a set of mutually orthogonal contrast vectors. For each variable, peak values arising from each regression line were averaged (expressed as means ± standard errors) and superimposed on the resulting plot. Statistical significance of differences was declared when $P < 0.05$.

Results

Morphological characteristics of the rats at sacrifice

PAH rats had lower body mass and tibial length than those of Control rats (Table 1). Lung dry mass and heart dry mass were significantly higher in PAH rats. The latter cohort developed RV hypertrophy and LV atrophy, as evident by the relative change of ventricular free wall thickness when normalised to heart mass. As shown in Table 2, the average lengths, cross-sectional areas and volumes of the LV and RV trabeculae were not different among groups.

Isometric contractions

Reduction of muscle length resulted in decreases of both steady-state active stress production and suprabasal heat output (Figure 1). The average relations of active stress-length and heat-length from either the LV (Figure 1D & E) or the RV (Figure 1G & H) trabeculae were not different between PAH and Control groups. As shown in Figure 2, RV trabeculae from PAH animals showed prolonged twitch duration and lower maximal rates of rise and fall of twitch stress, but no difference was detected in the area under the twitch-time profile (stress-time integral, STI). In contrast, normal isometric twitch kinetics obtained in the LV trabeculae.

Figure 3A shows steady-state twitch heat as a function of active stress arising from the two distinct protocols: 'work-loop' and 'pre-shortened isometric' contractions. The slopes of both heat-stress relations were lower for the PAH RV trabeculae (Figure 3D & E). The averaged heat-intercept of the isometric heat-stress relation (an index of activation heat) of RV trabeculae from PAH rats was significantly greater than that of their Control group, whereas no difference was detected in the LV trabeculae (Figure 3F). There was no difference in the averaged peak shortening heat between either groups or ventricles (Figure 3G).

Work-loop contractions

In Figure 5, work output, suprabasal enthalpy (work plus suprabasal heat) and suprabasal efficiency, quantified from Figure 4, are plotted as functions of relative afterload. Peak work output was significantly lower in RV trabeculae from PAH rats, despite there being no difference in suprabasal enthalpy; hence, suprabasal efficiency was lower compared to that of the Control group. However, when account was taken of the difference in activation heat (Figure 3E), crossbridge efficiency of RV trabeculae was revealed to be not significantly different between groups. In contrast, the LV trabeculae showed no difference in work, or in either suprabasal or crossbridge efficiency between two groups. Both extent and velocity of shortening as functions of relative active stress (Figure 6)

were significantly lower in the RV trabeculae from PAH rats compared with those of their respective Control groups, whereas no difference between groups was detected in the LV trabeculae for either relation.

Discussion

Overview We find that energy utilisation by trabeculae isolated from the hypertrophied RV in end-stage right-ventricular failure induced by PAH is indeed disturbed. PAH RV trabeculae developed the same active stress, but they have reduced extent and velocity of shortening. Thus their production of peak external work was reduced. Since they released the same amount of suprabasal enthalpy, their suprabasal efficiency was reduced. Whereas the component of myocardial efficiency attributed to crossbridge shortening was maintained, the component apportioned to the performance of stress-length work-loops was greatly reduced. Hence, their reduced suprabasal efficiency was due to the increased energy cost of the Ca^{2+}-triggered activation process. Surprisingly, despite the LV having undergone a period of atrophic remodelling, the ability of their trabeculae to utilise energy, and hence their energy efficiency, was unaffected.

Energetics of the right-ventricular trabeculae in PAH This is the first study to have examined the mechanoenergetic response of trabeculae in the PAH setting. We distinguished the energy used for Ca^{2+} cycling and that consumed by crossbridge cycling. Crossbridge cycling heat was further partitioned into shortening and non-shortening (isometric) components (Pham *et al.*, 2017a; Tran *et al.*, 2017). Separation of the energy demands of these two energy sinks clarifies the cellular mechanisms underlying disturbed energy utilisation in hypertrophied RV myocardium. Studies of human patients, and of the MCT-hypertensive rats, have provided ample evidence that the oxygen consumption of the hypertrophied RV myocardium is higher. As work output is unchanged, RV efficiency is thus lower in PAH (Wong *et al.*, 2010; Wong *et al.*, 2011). We extended these findings by showing that the PAH RV trabeculae require greater thermal expenditure for the Ca^{2+}-triggered activation of contractile events (Figure 3). This source of energy cost, coined 'activation heat' or 'Ca^{2+} cycling heat', is indexed by the heat-intercept of the isometric heat-stress relation (Hill, 1949; Gibbs *et al.*, 1967; Loiselle & Gibbs, 1979; Pham *et al.*, 2017b). It comprises the thermal accompaniment of the hydrolysis of ATP by the sarcoplasmic reticular Ca^{2+}-ATPase (SERCA) and the sarcolemmal Na^{+}-

K^+-ATPase, as well as the Na^+/Ca^{2+} exchanger (NCX) and the sarcolemmal Ca^{2+}-ATPase (Schramm *et al.*, 1994). We have recently shown that activation heat is independent of muscle length and hence muscle stress (Pham *et al.*, 2017b). The latter does not differ between PAH and Control trabeculae in either ventricle (Figure 1B & C). Nevertheless, PAH RV trabeculae demonstrated greater thermal expenditure associated with Ca^{2+}-triggered activation (Figure 3F). Our results align with literature findings on studies of RV failure showing impaired SR Ca^{2+} uptake (Endo *et al.*, 2006) with higher diastolic $[Ca^{2+}]_i$ and larger Ca^{2+} waves (Miura *et al.*, 2011).

Suprabasal enthalpy consists of activation heat and crossbridge enthalpy. Our finding of similar suprabasal enthalpy between RV groups (Figure 5F) cannot be directly compared with that of Wong *et al*. because their measurements of oxygen consumption of the whole hearts (Wong *et al.*, 2011) as well as papillary muscles (Wong *et al.*, 2010) necessarily included a basal component. These somewhat disparate results could be reconciled if future measurements were to show a higher rate of basal metabolism in the hypertrophic RV myocardium, possibly as a result of a higher rate of protein turnover (Everett *et al.*, 1977) in response to hypertrophy.

The lower peak work output of the PAH RV trabeculae does not stem from their inability to produce contractile stress, as they show the same development of isometric active stress as the Control group (Figure 1). Despite developing the same active stress, they reveal an increased passive stress-length relation, consistent with increased fibrosis in the RV myocardium in PAH (Daicho *et al.*, 2009; Handoko *et al.*, 2009). The PAH RV trabeculae also show prolonged twitch duration (Figure 2C), which has been attributed to prolongation of the action potential (Lee *et al.*, 1997; Piao *et al.*, 2010; Hardziyenka *et al.*, 2012), down-regulation of voltage gated K^+ channels (Piao *et al.*, 2010) and prolongation of the Ca^{2+} transient (Kuramochi *et al.*, 1994; Xie *et al.*, 2012; Lookin *et al.*, 2015). We note that comparable results of normal active stress production have been reported in isolated RV trabeculae (Kogler *et al.*, 2003) and papillary muscles (Wong *et al.*, 2010) from the same animal model under similar experimental conditions. However, previous studies have reported lower active stress in RV trabeculae from PAH tissues (Korstjens *et al.*, 2002; Miura *et al.*, 2011; Lookin *et al.*, 2015), and higher active stress in isolated permeabilised cardiomyocytes of RV tissue from PAH patients (Rain *et al.*, 2013). Whether such discrepancies can be attributed to differences of protocol or of experimental or environmental conditions awaits further exploration.

The failure of the PAH RV trabeculae to develop stress-length work as great as that of the Control group can be attributed to their inability to shorten to the same extent. Their lower extent of shortening arises from their reduced speed of shortening (Figure 6), consistent with the reported

shift in the myosin heavy chain isoform from predominantly V_1 to V_3 in the PAH model (Korstjens *et al.*, 2002; Kogler *et al.*, 2003; Hardziyenka *et al.*, 2011). Our findings of reduced extent and velocity of shortening are likewise consistent with data from PAH patients, obtained using echocardiography, showing reduced peak RV wall systolic strain and strain rate (Li *et al.*, 2013). Thus, the above comprehensive results extend previous observations by Wong *et al.* (2010), and imply that reduced work output, and increased thermal costs of the Ca^{2+}-triggered activation of contractile events are the main mechanisms underlying the reduction of suprabasal efficiency in PAH RV tissue.

Energetics of the left-ventricular trabeculae in PAH Our study has extended the investigation of the consequences of PAH-induced RV hypertrophy to include the atrophied LV myocardium. The LV myocardium in PAH, like the RV, also demonstrates a shift of MHC profile from the fast to the slow isoforms (Lowes *et al.*, 1997; Correia-Pinto *et al.*, 2009). Despite these reported MHC shifts, we find that the PAH LV trabeculae maintain both their extents and velocities of shortening. These results are consistent with those seen in human patients where the maximal velocities of contractile element shortening and circumferential fiber shortening are unaffected by chronic PAH (Krayenbuehl *et al.*, 1978).

We also find that PAH LV trabeculae are capable of developing normal stress (Figure 1), a result which is in agreement with that reported by Kogler *et al.* (2003). Their normal stress as a function of muscle length is associated with normal twitch kinetics (Figure 2). Hence, their work output is normal, and concomitantly, their heat output is also normal. Hence, both their suprabasal and crossbridge efficiencies remain normal (Figure 5).

Our null results of mechano-energetics changes in PAH LV trabeculae are somewhat unexpected. Our MCT-treated rats clearly suffered LV atrophy, as confirmed by a decrease in their normalised LV wall thickness (Table 1). Furthermore, in the same rat model (Kogler *et al.*, 2003; Umar *et al.*, 2012), as well as in patients (Hardziyenka *et al.*, 2011; Hardziyenka *et al.*, 2012), LV atrophic remodelling is manifested as impaired diastolic filling due to leftward interventricular septal bowing during contraction (Gan *et al.*, 2006). Electrophysiological alteration has also been shown to occur in the atrophic LV of both PAH patients and rats (Hardziyenka *et al.*, 2012). Despite these well-documented in changes in both animal models and human patients, we saw negligible effects of PAH on LV mechano-energetics.

Summary The null effect of PAH on crossbridge efficiency underscores our contention that the reduction of suprabasal efficiency in RV trabeculae arises largely from increased energy costs of Ca^{2+} cycling. The mechano-energetics of the LV myocardium remain preserved in PAH rats.

References

Campo A, Mathai SC, Le Pavec J, Zaiman AL, Hummers LK, Boyce D, Housten T, Champion HC, Lechtzin N, Wigley FM, Girgis RE & Hassoun PM. (2010). Hemodynamic predictors of survival in scleroderma-related pulmonary arterial hypertension. *Am J Respir Crit Care Med* **182,** 252-260.

Correia-Pinto J, Henriques-Coelho T, Roncon-Albuquerque R, Jr., Lourenco AP, Melo-Rocha G, Vasques-Novoa F, Gillebert TC & Leite-Moreira AF. (2009). Time course and mechanisms of left ventricular systolic and diastolic dysfunction in monocrotaline-induced pulmonary hypertension. *Basic Res Cardiol* **104,** 535-545.

Daicho T, Yagi T, Abe Y, Ohara M, Marunouchi T, Takeo S & Tanonaka K. (2009). Possible involvement of mitochondrial energy-producing ability in the development of right ventricular failure in monocrotaline-induced pulmonary hypertensive rats. *J Pharmacol Sci* **111,** 33-43.

Endo H, Miura M, Hirose M, Takahashi J, Nakano M, Wakayama Y, Sugai Y, Kagaya Y, Watanabe J, Shirato K & Shimokawa H. (2006). Reduced inotropic effect of nifekalant in failing hearts in rats. *J Pharmacol Exp Ther* **318,** 1102-1107.

Everett AW, Taylor RR & Sparrow MP. (1977). Protein synthesis during right-ventricular hypertrophy after pulmonary-artery stenosis in the dog. *Biochem J* **166,** 315-321.

Feldman HA. (1988). Families of lines: random effects in linear regression analysis. *J Appl Physiol* **64,** 1721-1732.

Gan CT, Lankhaar JW, Marcus JT, Westerhof N, Marques KM, Bronzwaer JG, Boonstra A, Postmus PE & Vonk-Noordegraaf A. (2006). Impaired left ventricular filling due to right-to-left ventricular interaction in patients with pulmonary arterial hypertension. *Am J Physiol Heart Circ Physiol* **290,** H1528-1533.

Gibbs CL, Mommaerts M & Ricchiuti NV. (1967). Energetics of cardiac contractions. *J Physiol* **191,** 25-46.

Goo S, Joshi P, Sands G, Gerneke D, Taberner A, Dollie Q, LeGrice I & Loiselle D. (2009). Trabeculae carneae as models of the ventricular walls: implications for the delivery of oxygen. *J Gen Physiol* **134,** 339-350.

Grundy D. (2015). Principles and standards for reporting animal experiments in The Journal of Physiology and Experimental Physiology. *J Physiol* **593,** 2547-2549.

Hadri L, Kratlian RG, Benard L, Maron BA, Dorfmuller P, Ladage D, Guignabert C, Ishikawa K, Aguero J, Ibanez B, Turnbull IC, Kohlbrenner E, Liang L, Zsebo K, Humbert M, Hulot JS, Kawase Y, Hajjar RJ & Leopold JA. (2013). Therapeutic efficacy of AAV1.SERCA2a in monocrotaline-induced pulmonary arterial hypertension. *Circulation* **128,** 512-523.

Han JC, Guild SJ, Pham T, Nisbet L, Tran K, Taberner A & Loiselle D. (2017). Left-ventricular energetics in pulmonary arterial hypertension-induced right-ventricular hypertrophic failure. *Front Physiol* **In press**.

Han JC, Taberner A, Kirton RS, Nielsen P, Archer R, Kim N & Loiselle D. (2011). Radius-dependent decline of performance in isolated cardiac muscle does not reflect inadequacy of diffusive oxygen supply. *Am J Physiol Heart Circ Physiol* **300,** H1222–H1236.

Handoko ML, de Man FS, Happe CM, Schalij I, Musters RJ, Westerhof N, Postmus PE, Paulus WJ, van der Laarse WJ & Vonk-Noordegraaf A. (2009). Opposite effects of training in rats with stable and progressive pulmonary hypertension. *Circulation* **120,** 42-49.

Hardziyenka M, Campian ME, Reesink HJ, Surie S, Bouma BJ, Groenink M, Klemens CA, Beekman L, Remme CA, Bresser P & Tan HL. (2011). Right ventricular failure following chronic pressure overload is associated with reduction in left ventricular mass: evidence for atrophic remodeling. *J Am Coll Cardiol* **57,** 921-928.

Hardziyenka M, Campian ME, Verkerk AO, Surie S, van Ginneken ACG, Hakim S, Linnenbank AC, de Bruin-Bon HACMR, Beekman L, van der Plas MN, Remme CA, van Veen TAB, Bresser P, de Bakker JMT & Tan HL. (2012). Electrophysiologic remodeling of the left ventricle in pressure overload-induced right ventricular failure. *J Am Coll Cardiol* **59,** 2193-2202.

Hill AV. (1949). The heat of activation and the heat of shortening in a muscle twitch. *Proc R Soc Lond B Biol Sci* **136,** 195–211.

Hsia HH & Haddad F. (2012). Pulmonary hypertension: a stage for ventricular interdependence? *J Am Coll Cardiol* **59,** 2203-2205.

Humbert M, Sitbon O, Chaouat A, Bertocchi M, Habib G, Gressin V, Yaïci A, Weitzenblum E, Cordier J-F, Chabot F, Dromer C, Pison C, Reynaud-Gaubert M, Haloun A, Laurent M, Hachulla E, Cottin V, Degano B, Jaïs X, Montani D, Souza R & Simonneau G. (2010). Survival in patients with idiopathic, familial, and anorexigen-associated pulmonary arterial hypertension in the modern management era. *Circulation* **122,** 156-163.

Johnston CM, Han JC, Ruddy BP, Nielsen PMF & Taberner AJ. (2015). A high-resolution thermoelectric module-based calorimeter for measuring the energetics of isolated ventricular trabeculae at body temperature. *Am J Physiol Heart Circ Physiol* **309,** H318-324.

Kogler H, Hartmann O, Leineweber K, Nguyen van P, Schott P, Brodde OE & Hasenfuss G. (2003). Mechanical load-dependent regulation of gene expression in monocrotaline-induced right ventricular hypertrophy in the rat. *Circ Res* **93,** 230-237.

Korstjens IJ, Rouws CH, van der Laarse WJ, Van der Zee L & Stienen GJ. (2002). Myocardial force development and structural changes associated with monocrotaline induced cardiac hypertrophy and heart failure. *J Muscle Res Cell Motil* **23,** 93-102.

Krayenbuehl HP, Turina J & Hess O. (1978). Left ventricular function in chronic pulmonary hypertension. *Am J Cardiol* **41,** 1150-1158.

Kuramochi T, Honda M, Tanaka K, Enomoto K, Hashimoto M & Morioka S. (1994). Calcium transients in single myocytes and membranous ultrastructures during the development of cardiac hypertrophy and heart failure in rats. *Clin Exp Pharmacol Physiol* **21,** 1009-1018.

Lamberts RR, Hamdani N, Soekhoe TW, Boontje NM, Zaremba R, Walker LA, de Tombe PP, van der Velden J & Stienen GJ. (2007). Frequency-dependent myofilament Ca^{2+} desensitization in failing rat myocardium. *J Physiol* **582,** 695-709.

Lee JK, Kodama I, Honjo H, Anno T, Kamiya K & Toyama J. (1997). Stage-dependent changes in membrane currents in rats with monocrotaline-induced right ventricular hypertrophy. *Am J Physiol* **272,** H2833-2842.

Li Y, Xie M, Wang X, Lu Q & Fu M. (2013). Right ventricular regional and global systolic function is diminished in patients with pulmonary arterial hypertension: a 2-dimensional ultrasound speckle tracking echocardiography study. *Int J Cardiovasc Imaging* **29,** 545-551.

Loiselle D & Gibbs CL. (1979). Species differences in cardiac energetics. *Am J Physiol* **237,** H90-H98.

Lookin O, Balakin A, Kuznetsov D & Protsenko Y. (2015). The length-dependent activation of contraction is equally impaired in impuberal male and female rats in monocrotaline-induced right ventricular failure. *Clin Exp Pharmacol Physiol* **42,** 1198-1206.

Lowes BD, Minobe W, Abraham WT, Rizeq MN, Bohlmeyer TJ, Quaife RA, Roden RL, Dutcher DL, Robertson AD, Voelkel NF, Badesch DB, Groves BM, Gilbert EM & Bristow MR. (1997). Changes in gene expression in the intact human heart. Downregulation of alpha-myosin heavy chain in hypertrophied, failing ventricular myocardium. *J Clin Invest* **100,** 2315-2324.

Marcus JT, Gan C, Zwanenburg JJ, Boonstra A, Allaart CP, Götte MJ & Vonk-Noordegraaf A. (2008). Interventricular mechanical asynchrony in pulmonary arterial hypertension: left-to-right delay in peak shortening is related to right ventricular overload and left ventricular underfilling. *J Am Coll Cardiol* **51,** 750-757.

Marcus JT, Vonk Noordegraaf A, Roeleveld RJ, Postmus PE, Heethaar RM, Van Rossum AC & Boonstra A. (2001). Impaired left ventricular filling due to right ventricular pressure overload in primary pulmonary hypertension: noninvasive monitoring using MRI. *Chest* **119,** 1761-1765.

Miura M, Hirose M, Endoh H, Wakayama Y, Sugai Y, Nakano M, Fukuda K, Shindoh C, Shirato K & Shimokawa H. (2011). Acceleration of Ca2+ waves in monocrotaline-induced right ventricular hypertrophy in the rat. *Circ J* **75,** 1343-1349.

Naeije R & Badagliacca R. (2017). The overloaded right heart and ventricular interdependence. *Cardiovasc Res* **113,** 1474-1485.

Pham T, Han JC, Taberner A & Loiselle D. (2017a). Do right-ventricular trabeculae gain energetic advantage from having a greater velocity of shortening? *J Physiol* **595,** 6477-6488.

Pham T, Tran K, Mellor KM, Hickey A, Power A, Ward ML, Taberner A, Han JC & Loiselle D. (2017b). Does the intercept of the heat-stress relation provide an accurate estimate of cardiac activation heat? *J Physiol* **595,** 4725-4733.

Piao L, Fang YH, Cadete VJ, Wietholt C, Urboniene D, Toth PT, Marsboom G, Zhang HJ, Haber I, Rehman J, Lopaschuk GD & Archer SL. (2010). The inhibition of pyruvate dehydrogenase kinase improves impaired cardiac function and electrical remodeling in two models of right ventricular hypertrophy: resuscitating the hibernating right ventricle. *J Mol Med (Berl)* **88,** 47-60.

Rain S, Handoko ML, Trip P, Gan CT, Westerhof N, Stienen GJ, Paulus WJ, Ottenheijm CA, Marcus JT, Dorfmuller P, Guignabert C, Humbert M, Macdonald P, Dos Remedios C, Postmus PE, Saripalli C, Hidalgo CG, Granzier HL, Vonk-Noordegraaf A, van der Velden J & de Man FS. (2013). Right ventricular diastolic impairment in patients with pulmonary arterial hypertension. *Circulation* **128,** 2016-2025, 2011-2010.

Redout EM, Wagner MJ, Zuidwijk MJ, Boer C, Musters RJ, van Hardeveld C, Paulus WJ & Simonides WS. (2007). Right-ventricular failure is associated with increased mitochondrial complex II activity and production of reactive oxygen species. *Cardiovasc Res* **75,** 770-781.

Schafer S, Ellinghaus P, Janssen W, Kramer F, Lustig K, Milting H, Kast R & Klein M. (2009). Chronic inhibition of phosphodiesterase 5 does not prevent pressure-overload-induced right-ventricular remodelling. *Cardiovasc Res* **82,** 30-39.

Schramm M, Klieber HG & Daut J. (1994). The energy expenditure of actomyosin-ATPase, Ca^{2+}-ATPase and Na^{+},K^{+}-ATPase in guinea-pig cardiac ventricular muscle. *J Physiol* **481,** 647-662.

Sitbon O, Humbert M, Nunes H, Parent F, Garcia G, Hervé P, Rainisio M & Simonneau Gé. (2002). Long-term intravenous epoprostenol infusion in primary pulmonary hypertension. *J Am Coll Cardiol* **40,** 780-788.

Taberner AJ, Han JC, Loiselle D & Nielsen PM. (2011). An innovative work-loop calorimeter for *in vitro* measurement of the mechanics and energetics of working cardiac trabeculae. *J Appl Physiol* **111,** 1798-1803.

Taberner AJ, Johnston CM, Pham T, June-Chiew H, Ruddy BP, Loiselle DS & Nielsen PM. (2015). Measuring the mechanical efficiency of a working cardiac muscle sample at body temperature using a flow-through calorimeter. In *IEEE Eng Med Biol Soc*, pp. 7966-7969.

Taberner AJ, Pham T, Han JC, Uddin R & Loiselle D. (2017). A flow-through infusion calorimeter for measuring muscle energetics during pharmacological interventions. In *IEEE I2MTC* pp. 1-5. Italy.

Tran K, Han JC, Crampin EJ, Taberner AJ & Loiselle DS. (2017). Experimental and modelling evidence of shortening heat in cardiac muscle. *J Physiol* **595,** 6313-6326.

Umar S, Lee JH, de Lange E, Iorga A, Partow-Navid R, Bapat A, van der Laarse A, Saggar R, Saggar R, Ypey DL, Karagueuzian HS & Eghbali M. (2012). Spontaneous ventricular fibrillation in right ventricular failure secondary to chronic pulmonary hypertension. *Circ Arrhythm Electrophysiol* **5,** 181-190.

van Wolferen SA, Marcus JT, Boonstra A, Marques KM, Bronzwaer JG, Spreeuwenberg MD, Postmus PE & Vonk-Noordegraaf A. (2007). Prognostic value of right ventricular mass, volume, and function in idiopathic pulmonary arterial hypertension. *Eur Heart J* **28,** 1250-1257.

Vonk-Noordegraaf A, Haddad F, Chin KM, Forfia PR, Kawut SM, Lumens J, Naeije R, Newman J, Oudiz RJ, Provencher S, Torbicki A, Voelkel NF & Hassoun PM. (2013). Right heart adaptation to pulmonary arterial hypertension: physiology and pathobiology. *J Am Coll Cardiol* **62,** D22-33.

Vonk-Noordegraaf A, Marcus JT, Gan CT, Boonstra A & Postmus PE. (2005). Interventricular mechanical asynchrony due to right ventricular pressure overload in pulmonary hypertension plays an important role in impaired left ventricular filling. *Chest* **128,** 628S-630S.

Wong YY, Handoko ML, Mouchaers KT, de Man FS, Vonk-Noordegraaf A & van der Laarse WJ. (2010). Reduced mechanical efficiency of rat papillary muscle related to degree of hypertrophy of cardiomyocytes. *Am J Physiol Heart Circ Physiol* **298,** H1190-1197.

Wong YY, Ruiter G, Lubberink M, Raijmakers PG, Knaapen P, Marcus JT, Boonstra A, Lammertsma AA, Westerhof N, van der Laarse WJ & Vonk-Noordegraaf A. (2011). Right ventricular failure in idiopathic pulmonary arterial hypertension is associated with inefficient myocardial oxygen utilization. *Circ Heart Fail* **4,** 700-706.

Wust RC, de Vries HJ, Wintjes LT, Rodenburg RJ, Niessen HW & Stienen GJ. (2016). Mitochondrial complex I dysfunction and altered NAD(P)H kinetics in rat myocardium in cardiac right ventricular hypertrophy and failure. *Cardiovasc Res* **111,** 362-372.

Xie YP, Chen B, Sanders P, Guo A, Li Y, Zimmerman K, Wang LC, Weiss RM, Grumbach IM, Anderson ME & Song LS. (2012). Sildenafil prevents and reverses transverse-tubule remodeling and Ca^{2+} handling dysfunction in right ventricle failure induced by pulmonary artery hypertension. *Hypertension* **59,** 355-362.

Competing Interests

None.

Author contributions

Conception and design of the work (TP, LN, AT, DL, J-CH); acquisition, analysis and interpretation of data (TP, LN, AT, DL, J-CH); and drafting the work (TP, DL, J-CH). All authors approved the final version of the manuscript and agree to be accountable for all aspects of the work in ensuring that questions related to the accuracy or integrity of any part of the work are appropriately investigated

and resolved, and all persons designated as authors qualify for authorship, while all those who qualify for authorship are listed.

Funding

This work was supported by the Heart Foundation of New Zealand: Project Grant 1601 (DL), Research Fellowship 1611 (J-CH) and Postgraduate Scholarship 1572 (TP), Marsden Fast-Start grant (15-UOA-209) from the Royal Society of New Zealand (J-CH, DL and AT), and Emerging Researcher First Grant (16/510) from the Health Research Council of New Zealand (J-CH).

Tables

Table 1. General characteristics of Control and MCT-treated PAH rats

Parameter	Control (n = 20)	PAH (n = 26)	
Body mass (g)	471.2 ± 6.0	395.5 ± 7.1	*
Tibial length (mm)	43.4 ± 0.04	40.0 ± 0.03	*
Lung dry mass (g)	0.27 ± 0.01	0.39 ± 0.03	*
Lung dry mass/Body mass (%)	0.057 ± 0.001	0.101 ± 0.008	*
Lung dry mass/Tibial length (g mm^{-1})	6.22 ± 0.15	9.15 ± 0.59	*
Heart dry mass (g)	0.29 ± 0.01	0.32 ± 0.01	*
Heart dry mass/Body mass (%)	0.061 ± 0.001	0.081 ± 0.002	*
Heart dry mass/Tibial length (g mm^{-1})	6.62 ± 0.15	7.45 ± 0.19	*
LV wall thickness (mm)	3.58 ± 0.07	3.39 ± 0.07	*
LV thickness/Heart dry mass (mm g^{-1})	12.59 ± 0.34	10.74 ± 0.30	*
RV wall thickness (mm)	1.52 ± 0.03	2.05 ± 0.06	*
RV thickness/Heart dry mass (mm g^{-1})	5.36 ± 0.18	6.48 ± 0.21	*

Value are means ± SE, *$P < 0.05$

Table 2. Trabeculae dimensions of Control and MCT-treated PAH rats

	LV trabeculae		RV trabeculae	
Parameter	**CON (n = 16)**	**PAH (n = 22)**	**CON (n = 14)**	**PAH (n = 21)**
Length (mm)	3.44 ± 0.15	3.50 ± 0.12	3.38 ± 0.12	3.03 ± 0.15
Cross-sectional area (mm^2)	0.070 ± 0.015	0.080 ± 0.009	0.072 ± 0.009	0.075 ± 0.007
Volume (mm^3)	0.24 ± 0.05	0.27 ± 0.03	0.25 ± 0.03	0.22 ± 0.02

Values are means ± SE; n, number of trabeculae.

Figure Legends

Figure 1: Results from the isometric pre-shortened protocol at 5 Hz. Typical experimental records of twitch stress (A) and rate of heat production (B) of a representative trabecula at various lengths (b-f) below its optimal length (a), where the insets depict single twitch, and where the dotted line segments were drawn to indicate the heat-rate baseline. The first force twitch at each muscle length depicts the rested-state contraction after the pause of stimulation, indicating the maximal post-rest potentiation of stress. Passive stress, active stress and active heat at steady state as functions of relative muscle length (L/L_o) for a single trabecula (C, F respectively) and for average relations of LV (D, G) and RV trabeculae (E, H) from Control (thin lines) and PAH (thick lines) rats. Data were fitted using third-order polynomials (in panels C-H). Data from panels C and F were obtained from an RV trabecula (length, 3.4 mm; cross-sectional area, 0.087 mm^2). Mean ± SEM values at optimal length (L_o). The star indicates $P < 0.05$ comparing the regression lines of PAH and Control groups.

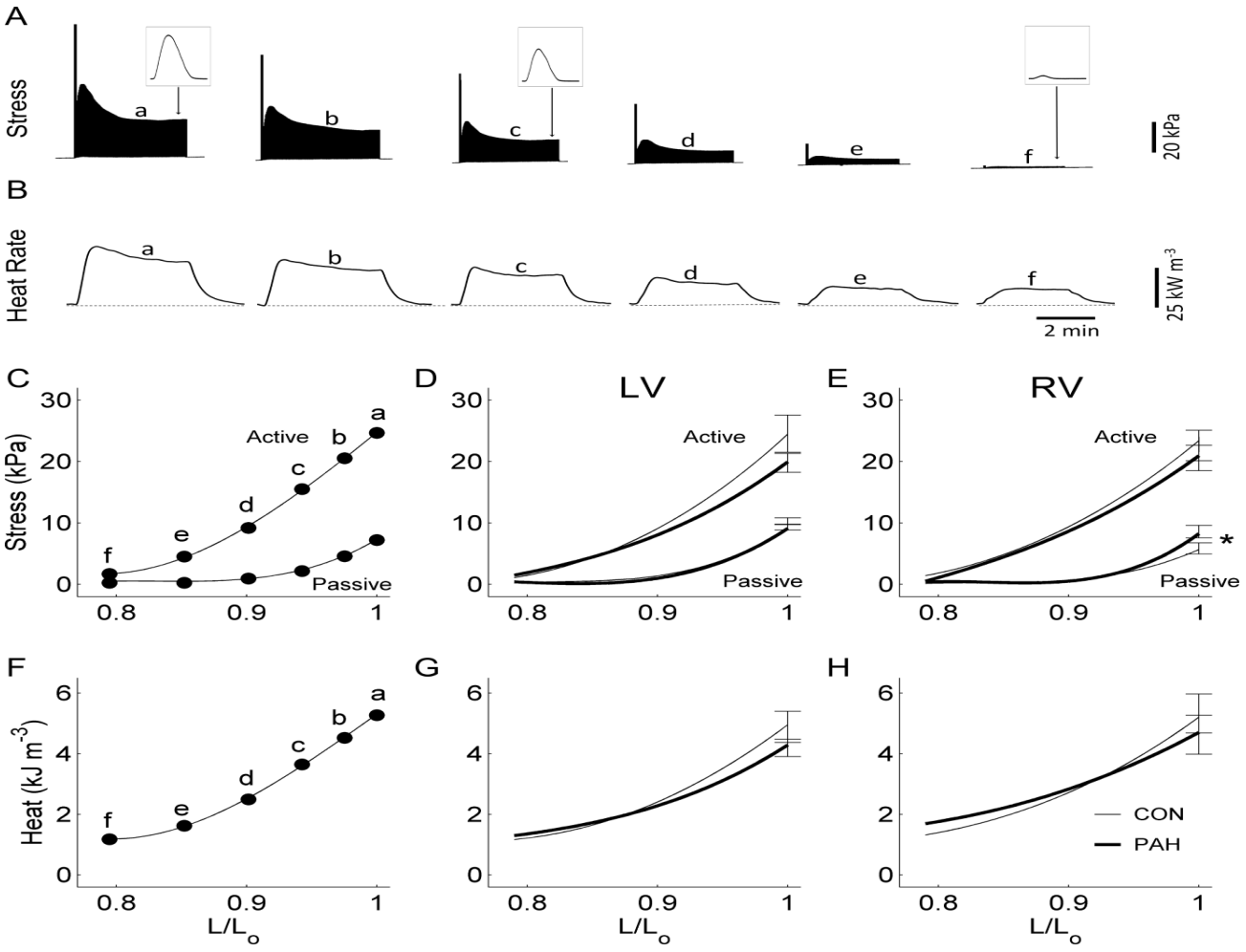

Figure 2: Temporal and kinetic characteristics of steady-state isometric twitches. Twitch duration at 5% (t_5) and at 50% (t_{50}) of peak stress, maximal rate of twitch stress development (+dS/dt, labelled 'rise') and relaxation (-dS/dt, labelled 'fall'), and stress-time integral (STI) as functions of active stress for a single trabecula (A, D, G) and for average LV (B, E, H) and RV trabeculae (C, F, I) from Control (thin lines) and PAH (thick lines) rats. Data were fitted using linear regressions in Panel A-F and second-order polynomials in Panel G-I. The data in panel A, D, G were obtained from an RV trabecula (length, 3.8 mm; cross-sectional area, 0.073 mm^2). The star indicates $P < 0.05$ comparing the regression lines of PAH and Control groups.

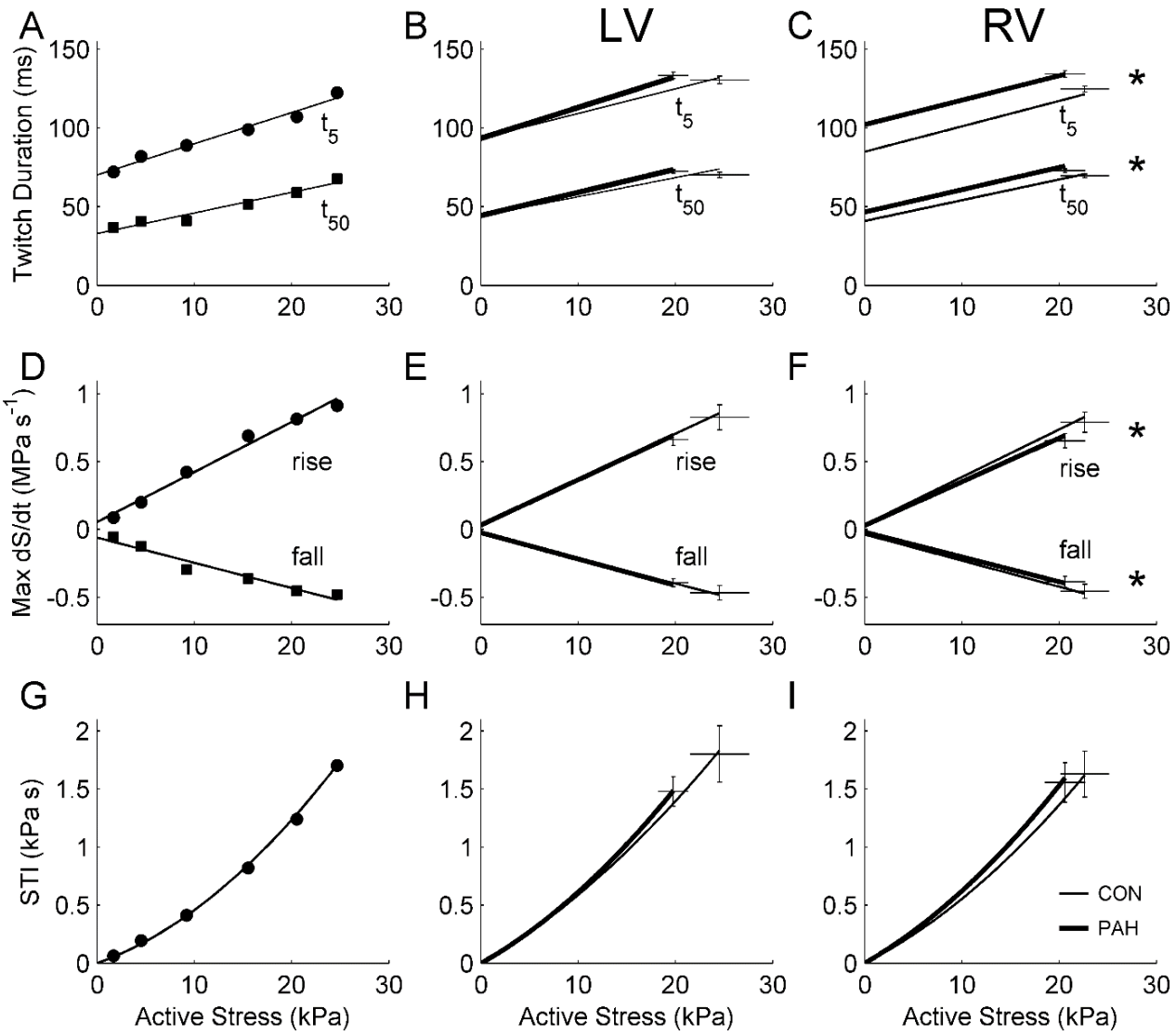

Figure 3: Twitch heat as functions of active stress for quantifying activation heat and shortening heat. (A) Linear regression of heat-stress relations arising from work-loop (open circles, broken lines) and isometric (filled circles, solid line) protocols for a representative trabecula and for the averages of LV trabeculae (B) and of RV trabeculae (C) from PAH (thick lines) and Control (thin lines) groups. The averaged values of the slopes were estimated from the heat-stress relations arising from both the isometric protocol (D) and the work-loop protocol (E). The averaged activation heat (Q_a, heat-intercepts of relations from the isometric protocol) was greater in the RV PAH group compared with their respective

Control group (F), as indicated by the star. Peak shortening heat (peak Q_s) was calculated as the difference between heat-intercepts from work-loop and isometric protocols (G). Representative data (Panel A) were from an RV trabecula (length, 3.8 mm; cross-sectional area, 0.073 mm^2).

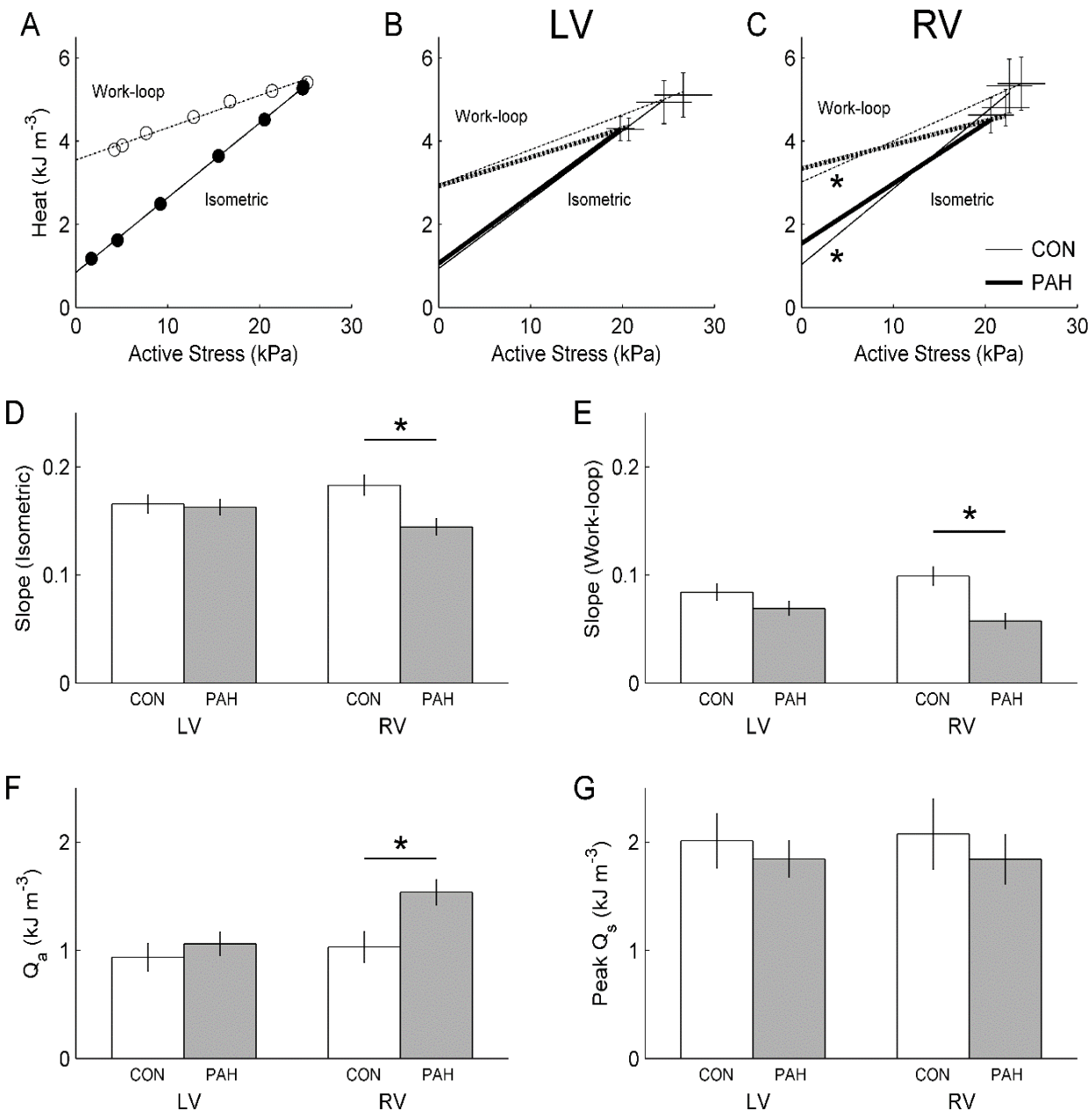

Figure 4: Typical experimental records arising from the work-loop protocol at 5 Hz. (A) Twitch stress of a trabecula undergoing progressively decreasing afterloaded work-loop contractions (b-g), bounded by return to isometric contractions at L_o (a). The first twitch illustrates the rested-state contraction immediately following the commencement of electrical stimulation. (B) The corresponding rates of heat output, where the dotted line is drawn to signify the heat-rate baseline. (C) Steady-state twitch stress profiles at various afterloads. (D) The corresponding steady-state muscle length

trajectory during each of twitch in Panel C. (E) Parametric plots of the stress and length profiles shown in C and D, resulting in stress-length work-loops. In all panels, data were obtained from an RV trabecula (length, 3.4 mm; cross-sectional area, 0.087 mm^2).

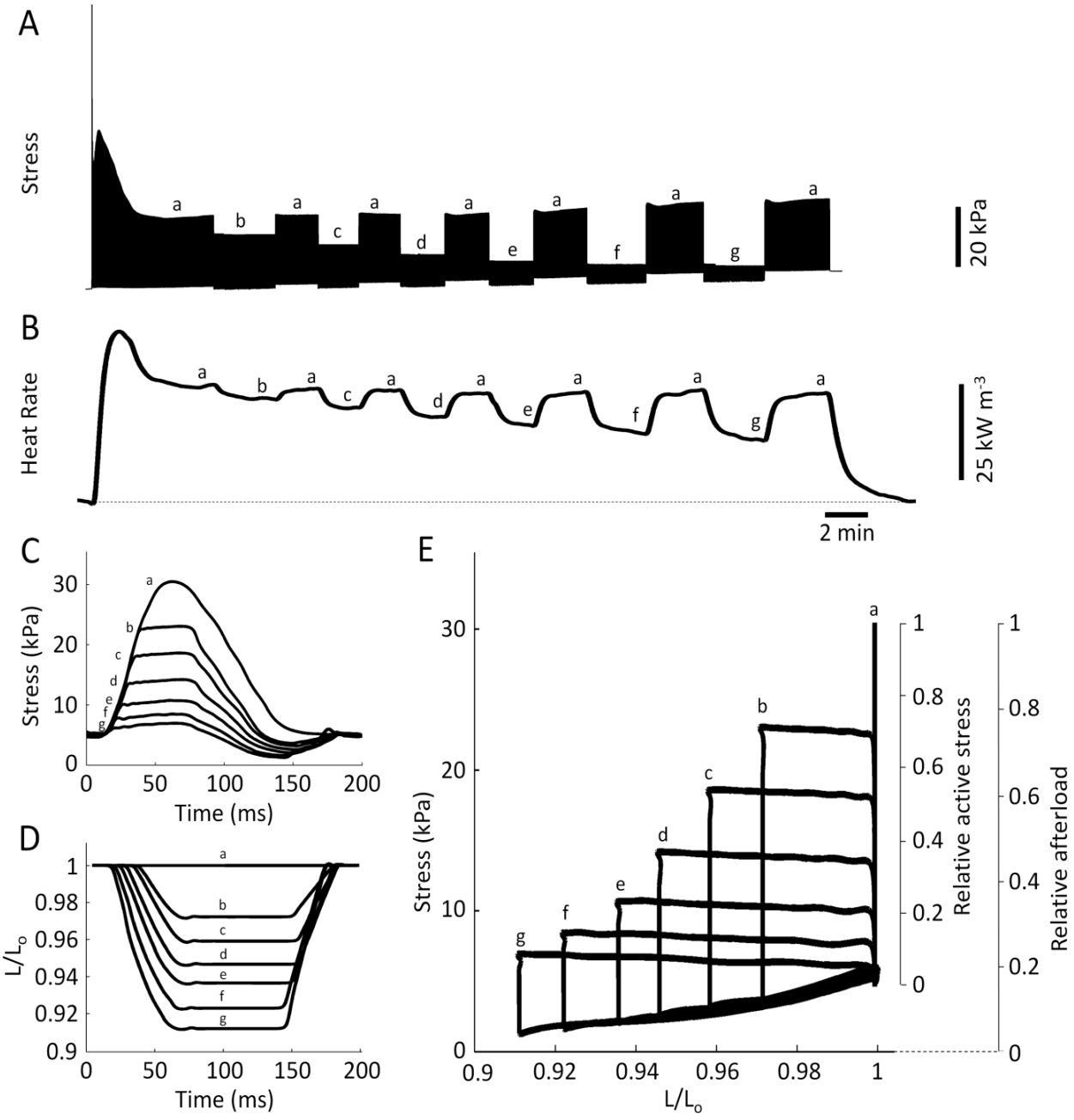

Figure 5: Energetics of afterloaded work-loop contractions at steady state. Data were fitted using second-order polynomials for enthalpy panels and third-order polynomials for the other panels. The left-most panels (A, D and G) show data from a single representative trabecula (length, 3.4 mm; cross-sectional area, 0.087 mm^2) whereas the middle panels (B, E and H) show averaged relations from the LV trabeculae and the right-most panels (C, F and I) show averaged relations

of the RV trabeculae. The data (panels A, D, G) were obtained from a RV trabecula. The star indicates $P < 0.05$ comparing the regression lines of PAH and Control groups.

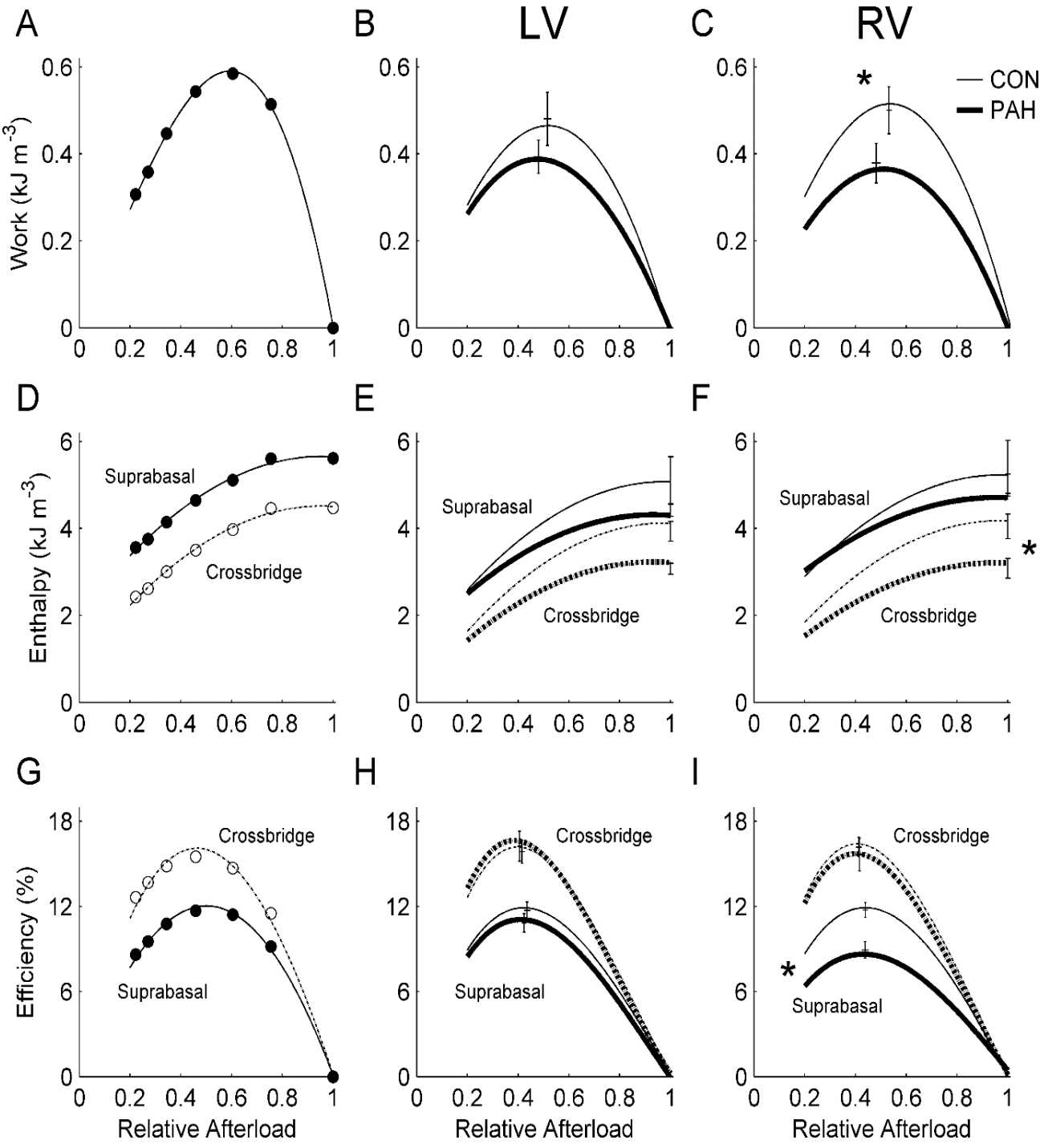

Figure 6: Shortening-related parameters arising from the work-loop protocol. Velocity of shortening and extent of shortening as functions of relative active stress for a single representative trabecula (A, D) of length 2.9 mm and cross-sectional area 0.035 mm^2, and for average relations of LV (B, E) and of RV trabeculae (C, F) from Control and PAH groups. SEM values were superimposed on the plots. The relations were lower for the RV PAH group compared with its Control group (as indicated by the star).

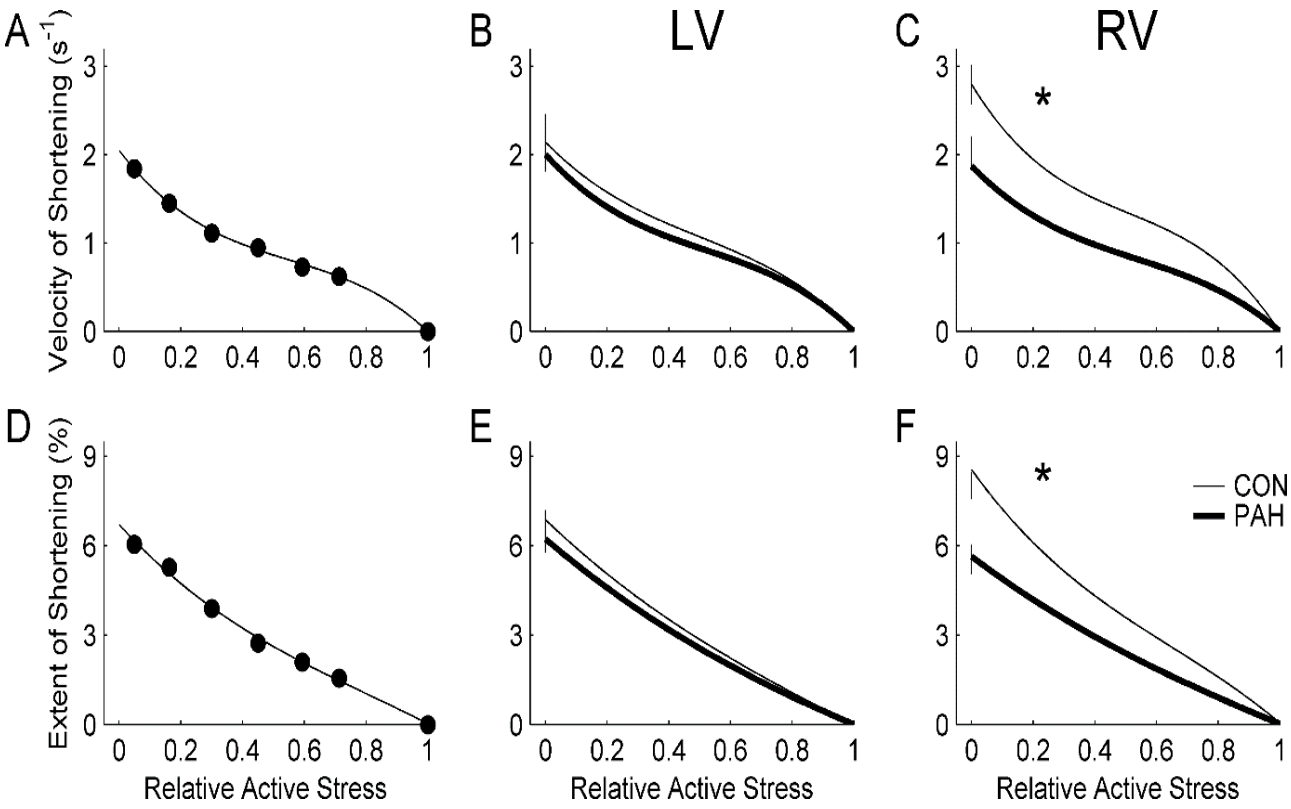

Figure 7: Variability of the data underlying Figure 5. Data were fitted using second-order polynomials for enthalpy panels and third-order polynomials for the other panels. Each panel shows individual data points, trabecula-specific regression

lines (LV-CON (n=16), LV-PAH (n=22), RV-CON (n=14), RV-PAH (n=21)), and the resulting averaged regression lines. Means ± SEMs of peak values were subsequently superimposed.